Collective plasmonic modes in ordered assemblies of metallic nanoshells

2008 J. Phys.: Condens. Matter 20 075232

(http://iopscience.iop.org/0953-8984/20/7/075232)

J. Phys.: Condens. Matter **20** (2008) 075232 (7pp) doi:10.1088/0953-8984/20/7/075232

Collective plasmonic modes in ordered assemblies of metallic nanoshells

C Tserkezis, G Gantzounis and N Stefanou

Section of Solid State Physics, University of Athens, Panepistimioupolis, GR-157 84 Athens, Greece

E-mail: ctserk@phys.uoa.gr

Received 30 November 2007, in final form 7 January 2008
Published 31 January 2008
Online at stacks.iop.org/JPhysCM/20/075232

Abstract

Collective plasmonic modes in two- and three-dimensional periodic assemblies of metallic nanoshells are studied by means of full electrodynamic calculations using the layer-multiple-scattering method. We consider structures made of a single type of nanoshell as well as binary heterostructures made of two different types of nanoshells. The complex photonic band structure of such three-dimensional photonic crystals is analyzed in conjunction with relevant transmission diagrams of corresponding finite slabs and the physical origin of the different optical modes is elucidated. Moreover, we discuss associated absorption spectra and provide a consistent interpretation of the underlying physics. In the case of the binary systems, the plasmonic modes of the two building components coexist, leading to a rich structure of resonances over an extended frequency range and to broadband absorption.

1. Introduction

Metallic nanoshells, particles with a dielectric core of diameter several tens of nanometers, covered with a metallic layer of few nanometers thickness, are being studied extensively in the recent years. This interest is motivated to a large extent by the tunability of plasmon resonances that these nanoparticles exhibit. Several methods have been developed for the fabrication of single nanoshells [1–4], as well as of periodic structures of such [5, 6]. Since these nanoparticles have a metallic component, they exhibit properties that stem from the excitation of surface plasmons, like large enhancement of the local field and strong light absorption. The combination of these properties with the tunability of resonances makes nanoshells promising candidates for a large variety of applications, such as surface enhanced Raman scattering [1, 7, 8], photonic band gap materials [9–11], waveguides [12], nanoantennas [13], solar spectrum harvesting [14], enhanced random lasing [15], medical applications [16], etc.

In this work, we report a theoretical study of the optical response of periodic structures of nanoshells using the on-shell layer-multiple-scattering method [17–19], which is ideally suited for photonic systems with absorptive and/or strongly dispersive constituents such as metallic materials. The method is effective when the structure under consideration consists of non-overlapping particles (scatterers) in a homogeneous host medium. The scattering properties of the individual particles enter only through the corresponding T matrix. For core–shell spheres, the scattering T matrix has an explicit analytic form [20]; however, here we evaluate it using a recursive formula for multiply coated spheres [21, 22]. In addition to the complex frequency band structure of a three-dimensional (3D) photonic crystal, associated with a given crystallographic plane, the layer-multiple-scattering method allows one to calculate, also, the transmission, reflection, and absorption coefficients of an electromagnetic (EM) wave incident at a given angle on a finite slab of the crystal and, therefore, it can describe an actual transmission experiment.

Throughout this paper, the optical response of the metallic material will be described by the simple Drude relative dielectric function [20]

$$\epsilon_{\mathrm{m}}(\omega) = 1 - \frac{\omega_{\mathrm{p}}^2}{\omega(\omega + \mathrm{i}\tau^{-1})}, \tag{1}$$

where ω_{p} is the bulk plasma frequency and τ the relaxation time of the conduction-band electrons, and $\mu_{\mathrm{m}} = 1$. For convenience, we shall express the frequency in units of ω_{p} and use c/ω_{p} as the length unit. We note that, considering a typical value 10 eV for $\hbar\omega_{\mathrm{p}}$, c/ω_{p} corresponds to about 20 nm.

The present paper is organized as follows. In section 2 we discuss aspects of the plasmon resonances in single metallic nanoshells, the emphasis being placed on the influence of

non-local effects. Section 3 deals with a two-dimensional (2D) periodic array of such nanoshells and, in particular, it examines the resonant excitation of collective plasmon modes by analyzing corresponding transmission and absorption spectra. In section 4 we report on the optical properties of a 3D photonic crystal of metallic nanoshells. More specifically, complementing previous theoretical work on the subject [11], we present a thorough group-theory analysis of the complex frequency band structure, in conjunction with relevant transmission diagrams of corresponding finite crystal slabs, and reveal the importance of the interacting plasmon modes. Section 5 is devoted to the study of binary heterostructures made of two different types of nanoshells. In particular, we describe how the plasmon modes of the building components lead to a rich structure of resonances over an extended frequency range and to a broadband absorption spectrum. Our results are summarized in section 6.

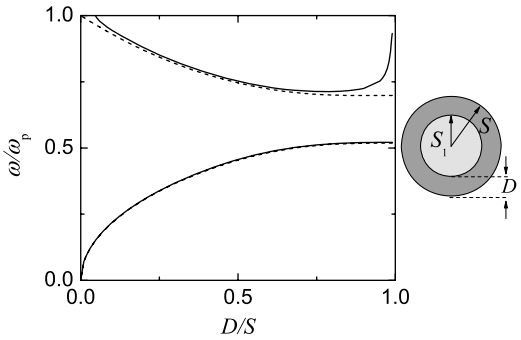

Figure 1. A core–shell spherical particle of radius S, consisting of a silica core of radius S_1 and a metallic shell of thickness D, in air. Variation of the location of the dipole-plasmon modes versus the shell thickness, taking into account the non-local correction (solid lines), if the particle radius is kept fixed at $S = c/\omega_p$. For comparison we also show the corresponding results when non-local corrections are neglected (dashed lines).

2. A single metallic nanoshell

The spectra of plasmon modes in metallic nanoshells are much richer than those in solid metallic nanoparticles, since particle plasmons (at the outer surface of the shell) and cavity plasmons (at the inner surface of the shell), both of electric 2^ℓ-pole type, can be concurrently excited. Moreover, the optical response of such nanoshells can be easily tuned by engineering their geometry. Plasmons of the outer and inner surfaces of the shell interact with each other and give rise to coupled modes, one below the lower (particle-like) and one above the higher (cavity-like) modes [23, 24]. The interaction and the resulting level shifts increase as the overlap between the corresponding wave fields becomes larger, i.e., by reducing the shell thickness, and is more pronounced for the dipole modes because of their relatively larger spatial extent. The effect is demonstrated in figure 1 for the dipole modes of a sphere of fixed radius $S = c/\omega_p$ consisting of a silica core ($\epsilon_{silica} = 2.1$, $\mu_{silica} = 1$) of radius S_1 coated with a metallic shell of thickness D. We have: $S_1 + D \equiv S = c/\omega_p$. In the absence of interaction between the two modes, i.e. for a vanishingly small core radius, the dipole particle-like plasmon mode is at $0.518\omega_p$ (the dipole-plasmon eigenfrequency of a homogeneous metallic particle of radius $S = c/\omega_p$ in air) and the dipole cavity-like plasmon mode at $0.698\omega_p$ (the dipole-plasmon eigenfrequency of a small silica sphere in a metal), as expected. As D decreases, the corresponding level shifts progressively increase.

In the case of very thin metallic shells, the electronic mean free path is shorter than in the bulk metal. This effect can be incorporated into the Drude dielectric function of equation (1), assuming a larger damping constant [25]:

$$\tau_S^{-1} = \tau^{-1} + \frac{1}{2}\left(\frac{3}{\pi}\right)^{1/3} v_F D^{-1}, \qquad (2)$$

where v_F is the Fermi velocity in the bulk metal.

On the other hand, non-local effects, which are associated with the excitation of longitudinal polarization waves in the nanoshell and a wavevector-dependent dielectric function, may also be non-negligible. Within the simple, yet effective, hydrodynamic model, the longitudinal dielectric function has the form:

$$\epsilon_L(q,\omega) = 1 - \frac{\omega_p^2}{\omega^2 - \frac{3}{5}v_F^2 q^2 + i\omega\tau^{-1}}, \qquad (3)$$

while the transverse dielectric function retains the simple local form of equation (1) [26]. The dispersion relation for the longitudinal plasma waves results from the condition $\epsilon_L(q_L,\omega) = 0$ implied by Maxwell's equations. Therefore, the expansion of the EM field into vector spherical waves within the nanoshell contains, in addition, longitudinal terms of the form $\nabla[Y_{\ell m}(\hat{\mathbf{r}})\, j_\ell(q_L r)]$ and $\nabla[Y_{\ell m}(\hat{\mathbf{r}})h_\ell^+(q_L r)]$, where $Y_{\ell m}$ are the usual spherical harmonics, and j_ℓ, h_ℓ^+ the spherical Bessel and Hankel functions, respectively. Imposing the boundary conditions of continuity of the tangential components of the electric and magnetic fields, as well as continuity of the radial component of the electric field at the (inner and outer) surfaces of the nanoshell, we obtain a system of linear equations for the field amplitudes that gives the scattering T matrix. The procedure is analogous to that in the corresponding case of a homogeneous metallic sphere [27]; however, in the present case, this procedure leads to relatively lengthy equations that we shall not write down explicitly here.

As shown by solid lines in figure 1, the non-local effects induce a blue shift of the dipole cavity-like plasmon resonances, in agreement with quasistatic calculations [28], while the corresponding particle-like resonances remain practically unchanged. This can be understood as follows. In the frequency region below ω_p, the longitudinal polarization field penetrates the nanoshell only in the form of evanescent waves, with an attenuation length which is inversely proportional to $\mathrm{Im}q_L$ and decreases as we move to lower frequencies. This evanescent field does however modify the internal field, thus causing a small shift of the resonance frequencies. In the low-frequency region of the dipole particle-like plasmon resonances, the penetration of the longitudinal field is obviously very small compared to the spatial extent of

these resonance modes and the interaction effect is negligibly small. On the contrary, the corresponding cavity-like modes have an appreciable overlap with the longitudinal wave field, since the latter has a larger penetration depth at higher frequencies. On the other hand, as the thickness of the nanoshell increases (large D) the localization of the cavity-like modes about the inner surface of the nanoshell becomes stronger, and therefore the interaction of these modes with the longitudinal field is more pronounced.

3. Two-dimensional periodic arrays

We consider a square array in the xy plane, with lattice constant $a_0 = 3c/\omega_p$, of the above core–shell particles with $S_1 = 0.7c/\omega_p$ and $D = 0.3c/\omega_p$, in air and neglect losses for now. The $(2\ell + 1)$ degeneracy of the resonant modes of the single metallic nanoshell is lifted because of the interaction with the other nanoshells of the plane. For $\mathbf{k}_\parallel = \mathbf{0}$ ($\mathbf{k}_\parallel$ is the xy component of the wavevector, $\mathbf{q}_\parallel$, reduced within the 2D surface Brillouin zone (SBZ)), the states of the EM field have the symmetry of the irreducible representations of the D_{4h} group: X_1, X_2, X_3, X_4, X_5, $X_{1'}$, $X_{2'}$, $X_{3'}$, $X_{4'}$ and $X_{5'}$ [29]. In agreement with a group-theory analysis, a dipole electric mode gives a $X_{4'}$ and a $X_{5'}$ mode, a quadrupole electric mode gives a X_1, a X_2, a X_3 and a X_5 mode, etc. Using the projection operator, we find that a plane EM wave propagating in the host region normal to the plane of nanoshells ($\mathbf{q}_\parallel = \mathbf{0}$) gives non-zero projection only to the representations of symmetry X_5 and $X_{5'}$, and therefore only modes of the plane of nanoshells with the same symmetry can be excited by an externally incident wave. The modes of different symmetry are inactive; they are bound states of the system and decay exponentially to zero away from the plane of nanoshells on either side of it. These inactive modes correspond to poles of the scattering S matrix [30] on the real frequency axis. Correspondingly, the optically active modes, of X_5 and $X_{5'}$ symmetry, correspond to poles of the S matrix in the lower complex frequency half-plane, with the imaginary part of the pole determining the inverse lifetime of the respective resonant mode. For example, the dipole particle-like plasmon mode of the single nanoshell gives a bound state of $X_{4'}$ symmetry at $0.416\omega_p$, and a $X_{5'}$ resonant state at $\omega_1 = 0.361\omega_p$ with an inverse lifetime $\gamma_1 = 0.040\omega_p$. On the other hand, the quadrupole particle-like plasmon mode of the nanoshell gives three bound states at $0.457\omega_p$ (X_2), $0.473\omega_p$ (X_1), $0.476\omega_p$ (X_3), and a X_5 resonant mode at $\omega_2 = 0.460\omega_p$ with an inverse lifetime $\gamma_2 = 8.3 \times 10^{-4}\omega_p$. Similarly, the dipole cavity-like plasmon mode of the single nanoshell gives a $X_{4'}$ bound state at $0.863\omega_p$, and a $X_{5'}$ resonant state at $\overline{\omega}_1 = 0.844\omega_p$ with an inverse lifetime $\overline{\gamma}_1 = 0.042\omega_p$. On the other hand, the quadrupole cavity-like plasmon mode of the nanoshell gives three bound states at $0.787\omega_p$ (X_3), $0.783\omega_p$ (X_1), $0.767\omega_p$ (X_2), and a X_5 resonant mode at $\overline{\omega}_2 = 0.769\omega_p$ with an inverse lifetime $\overline{\gamma}_2 = 2.9 \times 10^{-3}\omega_p$. With increasing ℓ, the eigenfrequencies of the particle- and cavity-like plasmon modes approach each other and give rise to a dense, almost continuous spectrum of eigenmodes.

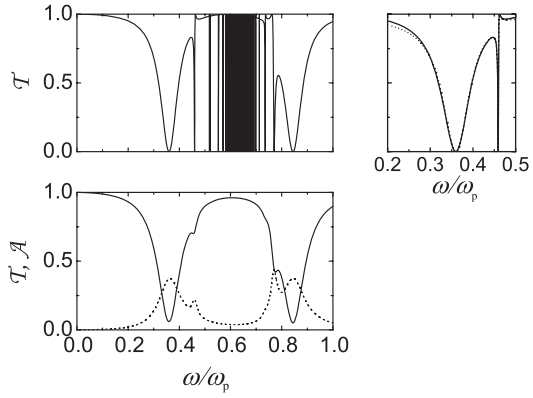

Figure 2. A square array, with lattice constant $a_0 = 3c/\omega_p$, of nanospheres, consisting of a silica core (radius $S_1 = 0.7c/\omega_p$) and a metallic shell (thickness $D = 0.3c/\omega_p$), in air. Upper panel: transmittance at normal incidence if absorption is neglected. A detailed view of the first two resonances is shown in the margin, together with a fit using equation (4) (dashed line). Lower panel: transmittance and absorbance at normal incidence if absorption in the metallic material is taken into account ($\tau^{-1} = 0.025\omega_p$).

In the upper panel of figure 2 we show the transmittance of the plane of non-absorbing nanoshells at normal incidence. It can be seen that the transmission spectrum is characterized by resonant structures of various types (Fano-like resonances) which originate from the corresponding resonant modes. If in a narrow region of frequency there is a number $i = 1, 2, \ldots$ of resonant states that correspond to poles of the S matrix at $\omega_i - i\gamma_i$ in the lower complex frequency half-plane, the transmittance has the form [31, 32]:

$$\mathcal{T} \approx \cos^2(\pm\delta_1 \pm \delta_2 \pm \ldots - \phi), \tag{4}$$

where $\sin\delta_i = \gamma_i[(\omega - \omega_i)^2 + \gamma_i^2]^{-1/2}$, $\cos\delta_i = -(\omega - \omega_i)[(\omega - \omega_i)^2 + \gamma_i^2]^{-1/2}$, and ϕ is an almost constant phase which contains the contributions of the non-resonant parts of the phase shifts. For example, up to $0.5\omega_p$, where there are, as mentioned above, two plasmon resonance states: $\omega_1 = 0.361\omega_p$, $\gamma_1 = 0.040\omega_p$ and $\omega_2 = 0.460\omega_p$, $\gamma_2 = 8.3 \times 10^{-4}\omega_p$, the calculated transmittance is very accurately reproduced by the function $\mathcal{T} = \cos^2(\delta_1 - \delta_2 - \phi)$, with $\phi = 178.4°$, as shown in the margin of the upper panel of figure 2. In general, the plasmon modes of the individual particles, in a 2D periodic arrangement, interact weakly between them and form relatively narrow bands, $\omega(\mathbf{k}_\parallel)$, of resonant modes about the corresponding eigenfrequencies of the single particle.

In the lower panel of figure 2 we show the transmittance and absorbance of the plane of nanoshells at normal incidence, taking into account dissipative losses in the metallic material ($\tau^{-1} = 0.025\omega_p$). We can see that the sharp features in the transmission spectrum, which originate from the resonant states with long lifetimes, are washed out by absorption, and essentially only the dipole and quadrupole plasmon modes manifest themselves in the transmittance. Correspondingly, the absorption spectrum is characterized by resonance peaks in the frequency regions of the above plasmon modes.

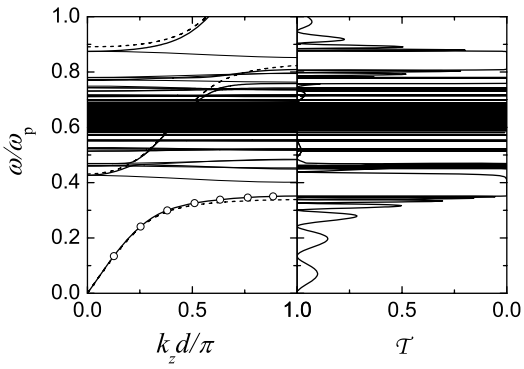

Figure 3. Left-hand panel: the photonic band structure of a fcc crystal, with lattice constant $a = 3\sqrt{2}c/\omega_p$, of non-absorbing nanospheres consisting of a silica core (radius $S_1 = 0.7c/\omega_p$) and a metallic shell (thickness $D = 0.3c/\omega_p$), in air, along the [001] direction. The thick and thin lines denote the doubly degenerate and non-degenerate bands, respectively, and the dashed lines show the results of the effective-medium approximation. Right-hand panel: transmittance at normal incidence of a slab of $N_L = 8$ (001) planes of the above crystal.

4. Three-dimensional crystals

We now consider a fcc crystal, built of a sequence of (001) planes of the above nanoshells. The crystal has a lattice constant $a = \sqrt{2}a_0 = 3\sqrt{2}c/\omega_p$ and the distance between successive (001) planes is $d = a/2$. We deliberately disregard absorption in the metallic material in order to be able to calculate the frequency band structure in an unambiguous manner. The left-hand panel of figure 3 shows the photonic band structure normal to the (001) surface. The symmetry of the bands along this direction (Δ_1, Δ_2, $\Delta_{1'}$, $\Delta_{2'}$, Δ_5) is that of the C_{4v} group [29]. The bands Δ_1, Δ_2, $\Delta_{1'}$, $\Delta_{2'}$ are non-degenerate and Δ_5 are doubly degenerate. We note that the (001) surface of the crystal under consideration is a plane of mirror symmetry and therefore the frequency bands appear in pairs: $k_z(\omega, \mathbf{k}_\parallel)$ and $-k_z(\omega, \mathbf{k}_\parallel)$; for this reason, in this figure we show the bands only for positive k_z.

At low frequencies we obtain a linear dispersion curve, of Δ_5 symmetry, as expected for propagation in a homogeneous medium characterized by a frequency-independent effective refractive index. At higher frequencies the band structure is dominated by flat, almost dispersionless bands which originate from the surface-plasmon modes of the nanoshells. With increasing ℓ, these resonance bands associated with the particle- and cavity-like plasmon modes of the individual nanoshells approach each other and give rise to a dense, almost continuous distribution of eigenmodes. The Δ_5 component of the resonance bands hybridizes with the extended Δ_5 band that would be in the effective medium to produce the Δ_5 bands in the photonic crystal shown in the left-hand panel of figure 3. It can be seen that frequency gaps open up due to hybridization between the extended band and flat bands with the same symmetry. The hybridization is stronger for the dipole resonance bands, because of the larger spatial extent of the associated wavefunctions, and the corresponding gaps are wider and well reproduced assuming a homogeneous effective medium characterized by $\mu_{\text{eff}} = 1$ and

$$\epsilon_{\text{eff}} = \frac{(qS)^3 - 3\mathrm{i}fT_{\text{E1}}(\omega)}{(qS)^3 + \frac{3}{2}\mathrm{i}fT_{\text{E1}}(\omega)}, \tag{5}$$

where f is the volume fraction occupied by the particles and T_{E1} is the electric dipole element of the T matrix [33], as shown by the dashed lines in the left-hand panel of figure 3. Interestingly, in the long-wavelength limit, equation (5) is equivalent to a two-step Maxwell-Garnett approximation, where an effective dielectric function ϵ_s is first obtained by homogenization of the individual coated particles:

$$\frac{\epsilon_s - \epsilon_m}{\epsilon_s + 2\epsilon_m} = \left(\frac{S_1}{S}\right)^3 \frac{\epsilon_{\text{silica}} - \epsilon_m}{\epsilon_{\text{silica}} + 2\epsilon_m}, \tag{6}$$

and then ϵ_s is used to calculate ϵ_{eff}:

$$\frac{\epsilon_{\text{eff}} - 1}{\epsilon_{\text{eff}} + 2} = f\frac{\epsilon_s - 1}{\epsilon_s + 2}. \tag{7}$$

The fine structure of the actual band diagram can be described by more elaborated effective-medium theories [11].

In the right-hand panel of figure 3 we show the transmittance of a slab of the crystal consisting of $N_L = 8$ (001) planes of nanoshells. The transmittance opposite the extended band exhibits the well-known Fabry–Perot oscillations due to multiple scattering between the surfaces of the slab. The period of these oscillations corresponds to $k_z d/\pi = 1/8$, as expected for the given slab thickness (see open circles in the left-hand diagram of figure 3). In the gap regions, and also within regions of frequency where only non-degenerate bands exist, the transmission coefficient practically vanishes.

The non-degenerate bands along the [001] direction arise from an apparently weak interaction between the corresponding bound states of the EM field, localized about consecutive (001) planes of scatterers. In order to demonstrate the above, we looked for the eigenmodes of the EM field, for $\mathbf{k}_\parallel = \mathbf{0}$, in a slab of $N_L = 8$ planes of nanoshells. Over the frequency range of each of these bands we obtain eight eigenfrequencies which, plotted against values of the reduced wavenumber $k_z = \kappa\pi/(N_L + 1)d$, $\kappa = 1, 2, \ldots, N_L$, ($N_L = 8$), reproduce the corresponding dispersion curves of the infinite crystal, as shown by the open circles in the left-hand panel of figure 4 for the lowest non-degenerate band. As discussed in section 3, the non-degenerate bands along the [001] direction of the crystal cannot be excited by an externally incident wave because they do not have the proper symmetry. However these bands survive for $\mathbf{k}_\parallel \neq \mathbf{0}$ (at least in the neighborhood of $\mathbf{k}_\parallel = \mathbf{0}$) where they couple with an incident wave of the same $\mathbf{k}_\parallel$ leading to measurable transmittance.

We note that the total number of bands shown in the left-hand panel of figure 3 equals the number expected from the degeneracy of the resonances of the individual nanoshells with a 'would be' extended effective-medium band. For example, as can be seen in the left-hand panel of figure 4, the dipole particle- and cavity-like plasmon modes of the individual nanoshells give a threefold degenerate state (of Γ_{15} symmetry)

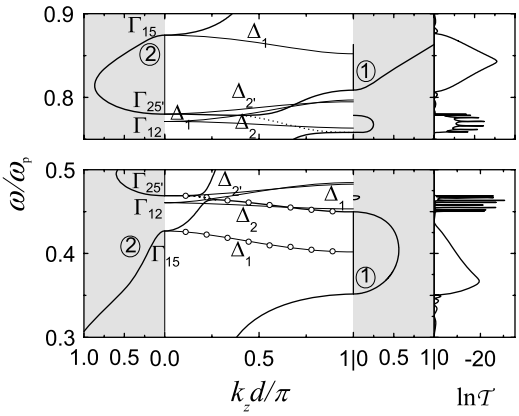

Figure 4. A detailed view of figure 3, in the frequency region of the dipole and quadrupole particle- and cavity-like plasmon modes. In the band structure diagram, apart from the ordinary frequency bands (k_z is real), we also show the real frequency lines for complex eigenvalues k_z which correspond to the doubly degenerate bands (the imaginary part of k_z is plotted in the gray-shaded areas). The corresponding transmission diagram is presented in logarithmic scale.

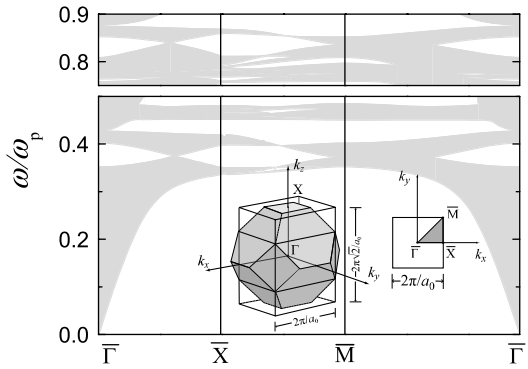

Figure 5. Projection of the photonic band structure of a fcc crystal, with lattice constant $a = 3\sqrt{2}c/\omega_p$, of non-absorbing nanospheres consisting of a silica core (radius $S_1 = 0.7c/\omega_p$) and a metallic shell (thickness $D = 0.3c/\omega_p$), in air, on the SBZ of the fcc (001) surface, along the symmetry lines shown in the inset.

at $\mathbf{k} = \mathbf{0}$ which is separated into a Δ_1 and a Δ_5 band along the [001] direction. The corresponding quadrupole modes give a threefold degenerate ($\Gamma_{25'}$) state and a doubly degenerate (Γ_{12}) state at $\mathbf{k} = \mathbf{0}$ which are separated into a $\Delta_{2'}$ and a Δ_5 band, and into a Δ_1 and a Δ_2 band along the [001] direction, respectively. Frequency gaps open up as a result of hybridization between the extended effective-medium band and the above Δ_5 resonance bands.

In the left-hand panel of figure 4, apart from the ordinary frequency bands (k_z is real), we also show the real frequency lines for complex eigenvalues k_z that correspond to the doubly degenerate bands. These lines are the analytic continuations in the complex k_z plane of the bands below and above the gaps [31]. The real frequency line of the appropriate symmetry (Δ_5 in the present case) with the smallest imaginary part over a frequency gap determines the attenuation of the wave field over this region; we obtain $\ln\mathcal{T}(\omega) = -2dN_L\mathrm{Im}[k_z(\omega)] + \text{const.}$, for a given value of $\mathbf{k}_\parallel$. This is indeed observed in the right-hand panel of figure 4, where we show the transmittance for a wave incident normally on a slab of the crystal consisting of $N_L = 8$ (001) planes. It can be seen that, in the region of the first gap, the real frequency line denoted by '1' determines the transmittance below $0.368\omega_p$ and that denoted by '2' determines the transmittance above $0.368\omega_p$. Similarly, in the gap extending from $0.808\omega_p$ to $0.875\omega_p$, the real frequency line denoted by '1' determines the transmittance below $0.843\omega_p$ and that denoted by '2' determines the transmittance above $0.843\omega_p$.

The resonance structures in the transmittance of the slab in the frequency region from $0.449\omega_p$ to $0.469\omega_p$ and $0.758\omega_p$ to $0.781\omega_p$ are clearly due to particle resonances localized about the individual layers interacting very weakly between them. It is worth noting the fact that the resonances of the slab appear at frequencies along the real frequency line corresponding to $\mathrm{Re}[k_z]d/\pi = \kappa/(N_L+1), \kappa = 1, 2, \ldots, N_L$, where $N_L = 8$ is the number of layers in the slab, as shown by the open circles in the lower diagram of the left-hand panel of figure 4. Which implies (and we have verified this numerically) that the number of transmission resonances increases with the thickness N_L of the slab.

In figure 5 we present the projection of the frequency band structure of the EM field of the photonic crystal under consideration on the symmetry lines of the SBZ of the fcc (001) surface. The shaded regions extend over the frequency bands of the EM field: at any one frequency within a shaded region, for given $\mathbf{k}_\parallel$, there exists at least one propagating EM mode in the infinite crystal. The blank regions represent frequency gaps for the given $\mathbf{k}_\parallel$. Obviously an absolute gap exists only when a blank region of frequency is common to all $\mathbf{k}_\parallel$ in the SBZ. We note that knowing the modes with $\mathbf{k}_\parallel$ in the shaded area ($\overline{\Gamma\mathrm{XM}}$) of the SBZ shown in the inset of figure 5 and $0 \leqslant k_z \leqslant \pi/d$ is sufficient for a complete description of all the modes in the infinite crystal. The modes in the remaining of the reduced $\mathbf{k}$ space are obtained through symmetry. One clearly sees that for the given crystal one does not obtain an omnidirectional frequency gap. This, according to our calculations, is also the case for corresponding crystals with different lattice constants.

5. Binary heterostructures

Since the eigenfrequencies of the plasmonic resonances of single metallic nanoshells vary drastically with D, it is interesting to investigate the optical response of complex structures, consisting for example of two types of metallic nanoshells of different thickness. In this case, one expects the coexistence of plasmonic resonances of both types of nanoshells in different regions of frequency. Based on the structure examined in section 4, we consider as unit a pair of consecutive (001) planes of the given fcc lattice, with the sites of the first plane occupied by silica core/metallic shell particles with $S_1 = 0.7c/\omega_p$ and $D = 0.3c/\omega_p$ (A), and the sites of the second plane occupied by silica core/metallic shell particles with $S_1 = 0.9c/\omega_p$ and $D = 0.1c/\omega_p$ (B). Repeating periodically this pair of planes, we build a binary structure AB

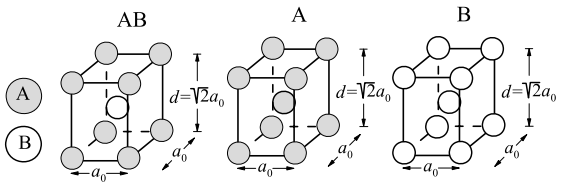

Figure 6. The unit cell of a tetragonal crystal AB of two different silica core/metallic shell particles: A ($S = c/\omega_p$, $D = 0.3c/\omega_p$) and B ($S = c/\omega_p$, $D = 0.1c/\omega_p$), together with the corresponding unit cells of fcc structures of the constituent components A and B.

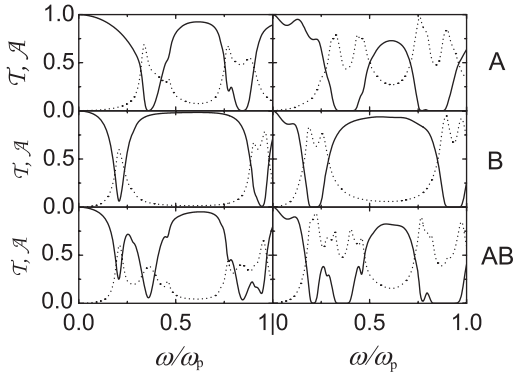

Figure 7. Transmittance (solid lines) and absorbance (dashed lines) at normal incidence of one (left-hand panel) and four (right-hand panel) pairs of consecutive (001) planes of the structures shown in figure 6. Dissipative losses in the metallic material are taken into account considering $\tau^{-1} = 0.025c/\omega_p$ in equation (1).

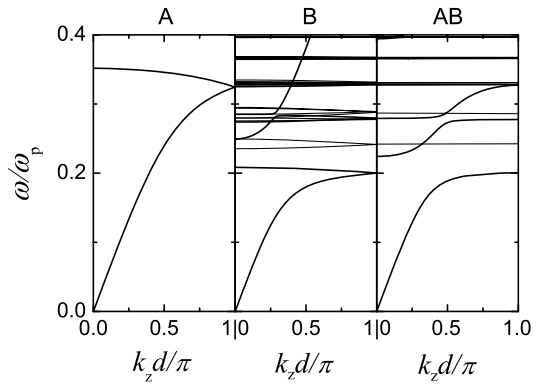

Figure 8. The photonic band structure of the crystals of figure 6, along the [001] direction.

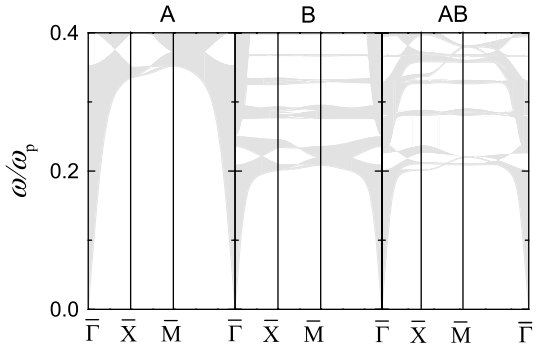

Figure 9. Projection of the photonic band structure of the crystals of figure 6 on the SBZ of the (001) surface, along the symmetry lines.

which is described by a tetragonal lattice of lattice constants a_0, and $\sqrt{2}a_0$, with the A particles at (000) and the B particles at $(\frac{1}{2}\frac{1}{2}\frac{1}{2})$, as shown in figure 6.

Figure 7 depicts the transmittance and absorbance at normal incidence for one and four pairs of such planes AB, together with the corresponding spectra when all planes are occupied either by nanoshells A or B, for comparison. It can be seen that the transmittance and absorbance exhibit resonance dips and peaks, respectively, that originate from both types of nanoshells. Obviously, the combination of two different nanoshells leads to strong, broadband absorbance.

Figure 8 displays the photonic band structure of the crystals of figure 6, neglecting losses in the metallic material, along the [001] direction, over a restricted frequency region. We note that the band diagram for crystal A in this figure is identical with the corresponding part of the diagram shown in the left-hand panel of figure 3. The only difference is that now we consider a unit cell twice as big as the fcc primitive cell, since $d = \sqrt{2}a_0$ here (see figure 6) while $d = \sqrt{2}a_0/2$ in section 4, and the bands are folded into the (smaller) Brillouin zone. The same reduced-zone representation also applies for crystal B, so that the results are directly comparable with those for crystal AB. The narrow bands originating from the surface-plasmon modes of the nanoshells, and the consequent gaps that result from hybridization of these bands with the extended effective-medium band, are shifted to lower frequencies in crystal B, compared with crystal A, because the nanoshells B are thinner than A. In crystal AB, the collective plasmonic modes of the two building components coexist. As can be seen in figure 8, we obtain in this case two sizable hybridization gaps along the [001] direction, about the eigenfrequencies of the dipole particle-like plasmon modes of both nanoshells A ($0.366\omega_p$) and B ($0.218\omega_p$). Interestingly, the $\ell = 4$ particle-like plasmon modes of the B component, and the associated flat bands, appear within the higher hybridization gap of crystal AB. However, the corresponding projections of the photonic band structures on the SBZ of the (001) surface, depicted in figure 9, show that there is no omnidirectional gap in these crystals. This finding, in conjunction with similar results reported in the literature [11], leads to the conclusion that photonic crystals of metallic nanoshells cannot easily exhibit sizable omnidirectional gaps in the optical region.

6. Conclusion

In conclusion, we reported a thorough theoretical study of the optical properties of 2D and 3D periodic structures of metallic nanoshells using the layer-multiple-scattering method. We find that the influence of non-local effects is appreciable only on the cavity-like plasmon resonances of ultrathin shells or nanoshells with a very small dielectric core. In assemblies of metallic nanoshells, the plasmon resonances of the individual particles interact weakly between them and form narrow bands of collective plasmon modes that manifest themselves as resonance structures in corresponding transmission spectra

and induce strong absorption. Such narrow bands, in 3D photonic crystals of metallic nanoshells, interact with the extended effective-medium band and frequency gaps open up as a result of this hybridization. However, these gaps are not, in general, omnidirectional. In the case of binary heterostructures, collective plasmonic modes originating from the two building components, which can be easily tuned by a proper choice of nanoshells, coexist, leading to hybridization gaps, broadband absorption, and a rich structure of resonances over an extended range of frequencies.

Acknowledgment

This work was supported by the research program 'Kapodistrias' of the University of Athens.

References

[1] Barnickel P and Wokaun A 1989 *Mol. Phys.* **67** 1355
[2] Zhou H S, Honma I, Komiyama H and Haus J W 1994 *Phys. Rev.* B **50** 12052
[3] Oldenburg S J, Averitt R D, Westcott S L and Halas N J 1998 *Chem. Phys. Lett.* **288** 243
[4] Romanov S G, Susha A S, Torres C M S, Liang Z and Caruso F 2005 *J. Appl. Phys.* **97** 086103
[5] Graf C and van Blaaderen A 2002 *Langmuir* **18** 524
[6] Zhan P, Liu J B, Dong W, Dong H, Chen Z, Wang Z L, Zhang Y, Zhu S N and Ming N B 2005 *Appl. Phys. Lett.* **86** 051108
[7] Kerker M and Blatchford C G 1982 *Phys. Rev.* B **26** 4052
[8] Jackson J B, Westcott S L, Hirsch L R, West J L and Halas N J 2003 *Appl. Phys. Lett.* **82** 257
[9] Zhang W, Wang Z, Hu A and Ming N 2000 *J. Phys.: Condens. Matter* **12** 9361
[10] Yannopapas V, Modinos A and Stefanou N 2002 *Opt. Quantum Electron.* **34** 227
[11] Li J, Sun G and Chan C T 2006 *Phys. Rev.* B **73** 075117
[12] Wang S M, Xiao J J and Yu K W 2007 *Opt. Commun.* **279** 384
[13] Wang H, Fu K, Drezek R A and Halas N J 2006 *Appl. Phys.* B **84** 191
[14] Cole J R and Halas N J 2006 *Appl. Phys. Lett.* **89** 153120
[15] Kang J U 2006 *Appl. Phys. Lett.* **89** 221112
[16] Hirsch L R, Gobin A M, Lowery A R, Tam F, Drezek R A, Halas N J and West J L 2006 *Ann. Biomed. Eng.* **34** 15
[17] Stefanou N, Karathanos V and Modinos A 1992 *J. Phys.: Condens. Matter* **4** 7389
[18] Stefanou N, Yannopapas V and Modinos A 1998 *Comput. Phys. Commun.* **113** 49
[19] Stefanou N, Yannopapas V and Modinos A 2000 *Comput. Phys. Commun.* **132** 189
[20] Bohren C F and Huffman D R 1983 *Absorption and Scattering of Light by Small Particles* (New York: Wiley)
[21] Wu Z S and Wang Y P 1991 *Radio Sci.* **26** 1393
[22] Tserkezis C 2005 *Diploma Dissertation* University of Athens
[23] Prodan E, Radloff C, Halas N J and Nordlander P 2003 *Science* **302** 419
[24] Teperik T V, Popov V V and Garcia de Abajo F J 2004 *Phys. Rev.* B **69** 155402
[25] Kraus W A and Schatz G C 1983 *J. Chem. Phys.* **79** 6130
[26] Jackson J D 1975 *Classical Electrodynamics* (New York: Wiley)
[27] Ruppin R 1975 *Phys. Rev.* B **11** 2871
[28] Chang R and Leung P T 2006 *Phys. Rev.* B **73** 125438
[29] Cornwell J F 1969 *Group Theory and Electronic Energy Bands in Solids* (Amsterdam: North-Holland)
[30] Gantzounis G, Stefanou N and Yannopapas V 2005 *J. Phys.: Condens. Matter* **17** 1791
[31] Gantzounis G and Stefanou N 2005 *Phys. Rev.* B **72** 075107
[32] Sainidou R and Stefanou N 2006 *Phys. Rev.* B **73** 184301
[33] Ruppin R 2000 *Opt. Commun.* **182** 273